Friedel *et al. GeoEnergy Communications* (2026) 2:8
https://doi.org/10.1007/s44421-026-00019-4

GeoEnergy Communications

RESEARCH Open Access

A novel approach to measure direct tensile strength on short-length cylindrical samples

M. Friedel[1], Y. Dong[1,2*], H. Konietzky[1], A. Morgenstern[1] and T. Wilsnack[3]

Abstract
The determination of tensile strength via direct tensile tests sets special requirements to the sample geometry. Under certain circumstances these requirements cannot be fulfilled. The proposed new lab test approach allows to perform direct tensile tests on short-length cylindrical homogeneous samples, but especially on samples with interfaces. The proposed procedure is verified by numerical simulations. Validation is documented exemplary for a homogeneous sandstone sample and a composite sample with interface (salt rock and special concrete).

Keywords Direct tensile test, Tensile strength, Lab testing, Short-length cylindrical samples, Interface tensile strength, Composite materials

1 Introduction

Tensile strength is an important strength parameter in rock mechanics and rock engineering [1, 2]. The direct tensile test is the most accurate method to determine the tensile strength of rocks [3, 4]. Other methods, like for instance Brazilian tests [5–9] or 3-point-bending tests [10, 11], which are easier to perform and therefore more popular, deliver also tensile strength values, but they are not that accurate. They are mostly slightly higher and therefore not conservative. Direct tensile testing typically requires specially designed loading devices [12, 13] to ensure stable force transmission and uniform stress distribution at the specimen ends, along with strict requirements on specimen dimensions [14]. In established direct tensile procedures for cylindrical rock core specimens, the specimen ends are commonly bonded to loading fixtures and connected to the testing machine through seating/linkage elements to minimize bending and torsion (ISRM suggested method [15], ASTM D2936-20 [16]; see also the multi-laboratory benchmark by Pérez-Rey et al. [17]). These setups are effective when specimen length and end preparation can be ensured. However, they can be difficult to apply to (i) short cores with length-to-diameter ratios close to unity and (ii) composite specimens containing an axial interface or weak plane, where end-capping and alignment may be impractical or may constrain the intended failure plane. The clamp-based procedure proposed here is intended as a practical extension of the ISRM/ASTM direct tension concept for these specific sample constellations rather than a replacement of standard direct tensile setups. Under some circumstances these demands cannot be fulfilled, for instance (a) the required sample length cannot be met (sample too short) or (b) the sample consists of two different materials along the long axis of the sample or (c) an interface or weak plane exist along the long axis. In these cases the new procedure described within this paper can be applied.

*Correspondence:
Y. Dong
dongyangokk@gmail.com
[1]TU Bergakademie Freiberg, Geotechnical Institute, Freiberg, Germany
[2]School of Environment and Architecture, University of Shanghai for Science and Technology, Shanghai, China
[3]IBEWA GmbH, Freiberg, Germany

2 Equipment description

The direct tensile testing apparatus employed for this study consists of an uniaxial tensile testing system supplemented by custom-designed metal clamps. The uniaxial tensile machine provides a precisely controlled axial tensile force, while the metal clamps (fixtures) ensure a uniform force transmission to the specimen throughout the loading process.

Figure 1 shows the used testing machine (a combined compression/tensile testing machine) with the following specifications for tensile tests:

- Tensile speed: adjustable within the range of 0.001–5 mm/min.
- Maximum tensile force: 100 kN.
- Measurement accuracy: ± 0.5% of full-scale range.

To overcome the specific limitations of the traditional direct tensile test method and to expand the test capabilities for certain sample constellations, a novel clamp (sampling holder) system is proposed as shown in Fig. 2. The clamp system consists of two symmetrical metal clamps, each featuring a semi-circular groove to securely hold the cylindrical specimen. During loading, this design ensures stable and uniform tensile force transmission. During loading, this design ensures stable and uniform tensile force transmission and reduces end effects compared with direct gripping; however, for homogeneous specimens some stress heterogeneity near the clamps may still occur and is discussed in Sect. 4 (see also Fig. 3). The semi-circular groove design not only minimizes potential specimen misalignment but also provides a large bonding (glue) area with identical adhesive tensile strength. The bonding strength of the glue (interface between rock sample and metal clamps) should be significantly higher than the rock strength. The inner radius of the metal clamps should be about 1 mm larger than those of the rock samples, which requires a thickness of the glue of 1 mm. The adhesive layer is an integral part of the load-transfer path between the specimen and the clamps. In the present setup, a nominal glue thickness of approximately 1 mm is defined by the clamp–specimen geometry. A structural epoxy was selected to provide high bond strength and sufficient stiffness, and to minimize

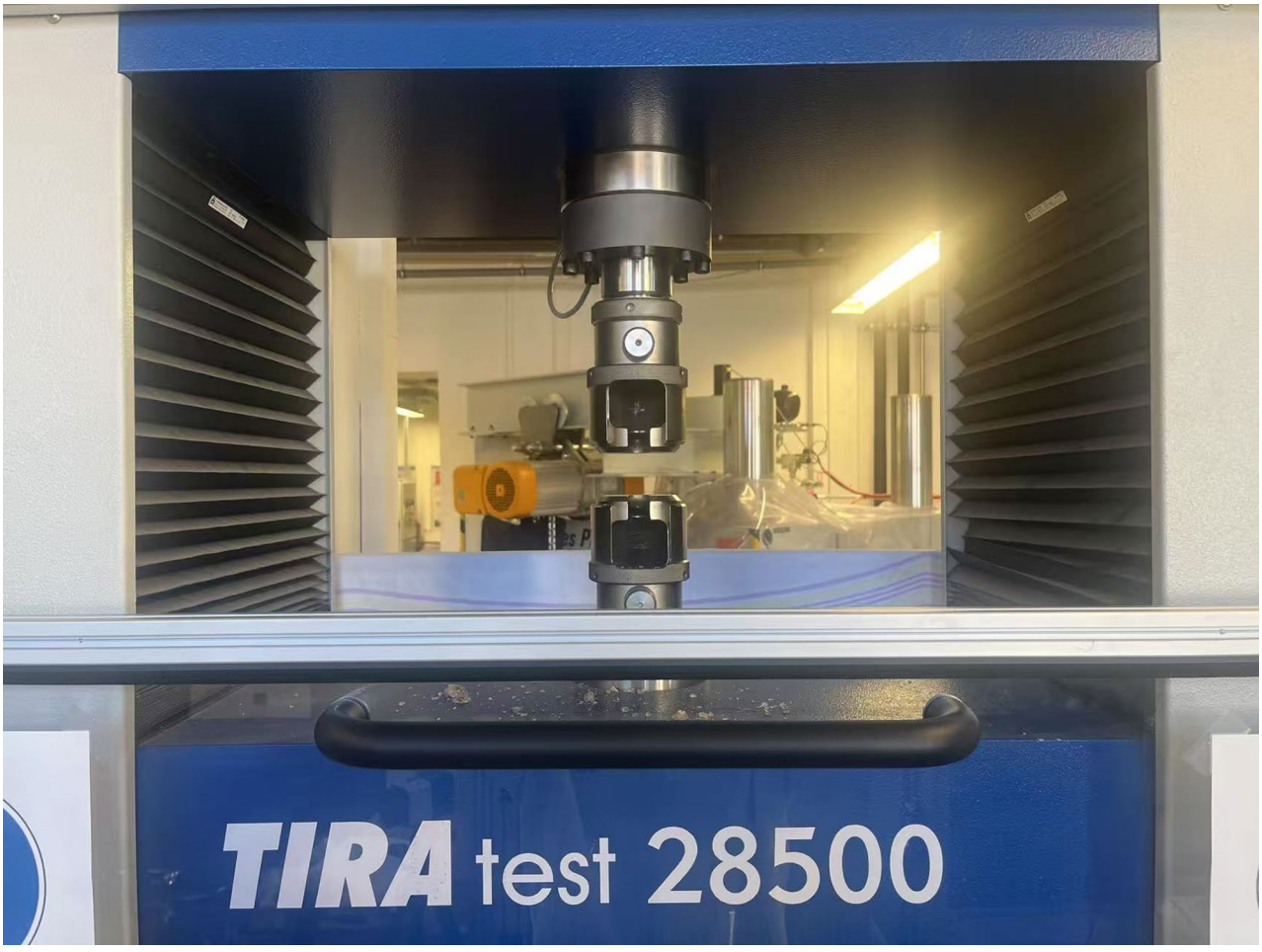

Fig. 1 Compression/tensile testing machine TIRAtest-2800

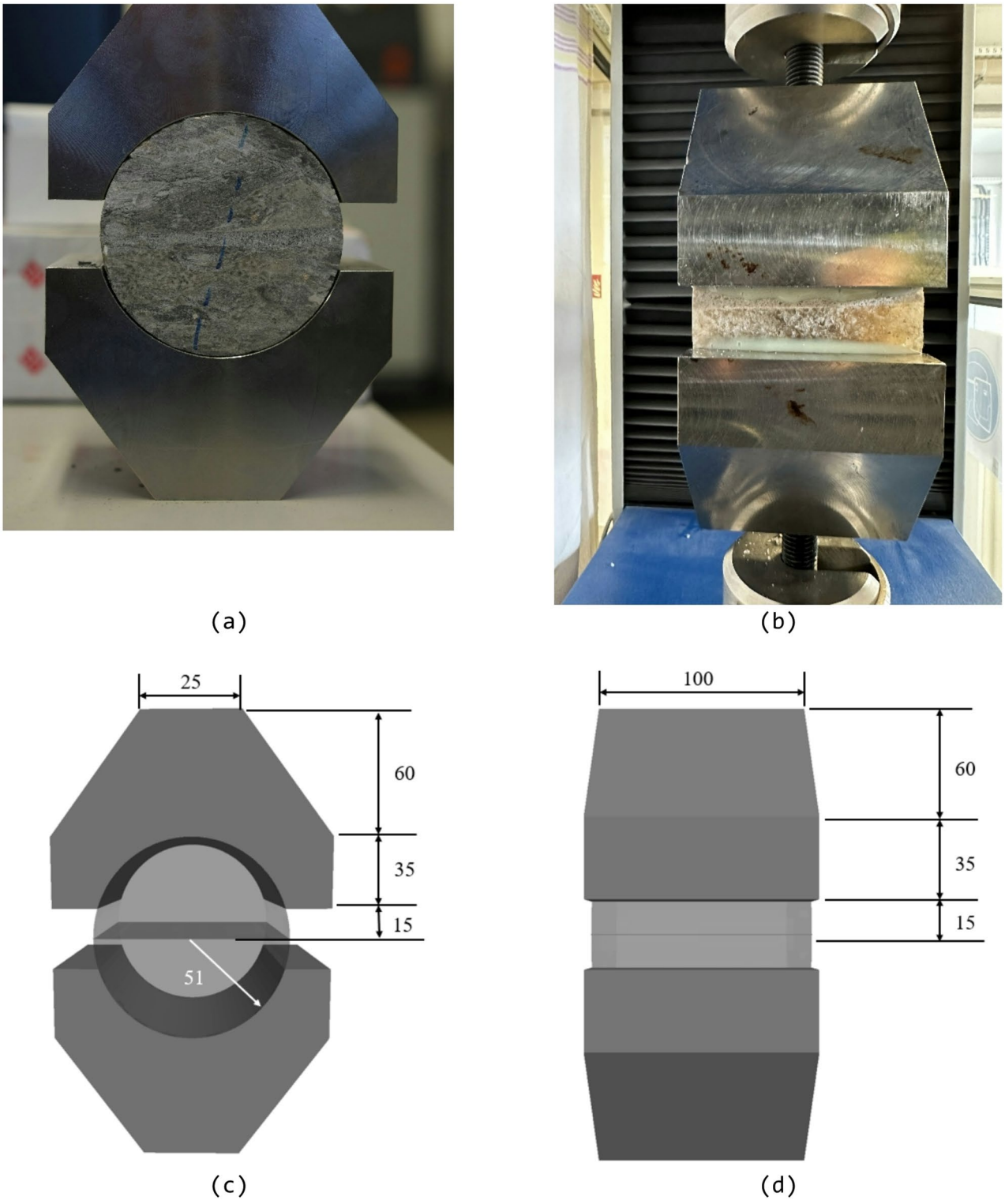

Fig. 2 Metal clamps. **a**, **b** Photograph of metal clamps, (**c**, **d**) Schematic of clamp design [mm]

time-dependent effects under the applied loading rates. Variations in adhesive thickness and stiffness mismatch may influence stress transfer and the magnitude of end effects; therefore, careful control of bonding procedure, curing conditions, and alignment is essential for reproducible results.

The clamps are fabricated from high-strength alloy steel, selected for its superior mechanical properties and

corrosion resistance. The key material specifications are as follows:

- Elastic modulus: $E = 200$ GPa (ensuring sufficient stiffness to minimize clamp deformation and its impact on test results).
- Yield strength: > 1000 MPa (preventing plastic deformation under maximum load conditions).
- Corrosion resistance: Suitable for various experimental environments, preventing degradation due to oxidation (corrosion) or impact by acids.

The specimen dimensions (cores with 100 mm diameter) used for our system are illustrated in Fig. 3. To ensure optimal bonding quality, the specimens are adhered to the metal clamps using a high-strength structural adhesive. The adhesive used must exhibit high bond strength, excellent durability, and negligible creep properties to prevent failure during testing. In this study, Hysol® 9466™ industrial grade epoxy adhesive was selected. Once mixed, the two component epoxy cures at room temperature to form a tough, off-white bondline which provides high peel resistance and high shear strength. The fully cured epoxy is resistant to a wide range of chemicals and solvents, and acts as an excellent electrical insulator. The Hysol® 9466™ glue has the following properties:

- Tensile strength: > 40 MPa.
- Shear strength: > 25 MPa.
- Curing time: 24–48 h.
- Operating temperature range: -40 °C to + 150 °C.
- Young's modulus: 3.2 GPa.
- Shear modulus: 1.1 GPa.

After the bonding process, specimens are cured in a controlled temperature environment for at least 24 h to ensure complete adhesive polymerization and development of maximum bond strength. Once cured, the specimen–clamp assembly is installed into the testing machine using ball-bearing mounted bolts, ensuring precise alignment of the loading direction with the specimen axis. This alignment is critical to eliminate bending or torsional loads. Prior to monotonic tensile loading, the assembly is seated under a small pre-load to ensure full contact and self-alignment of the linkage. The symmetric clamp geometry and the axial ball-bearing connection help to minimize eccentricity.

Upon test completion, to facilitate fixture reuse, the components with residual epoxy adhesive were placed

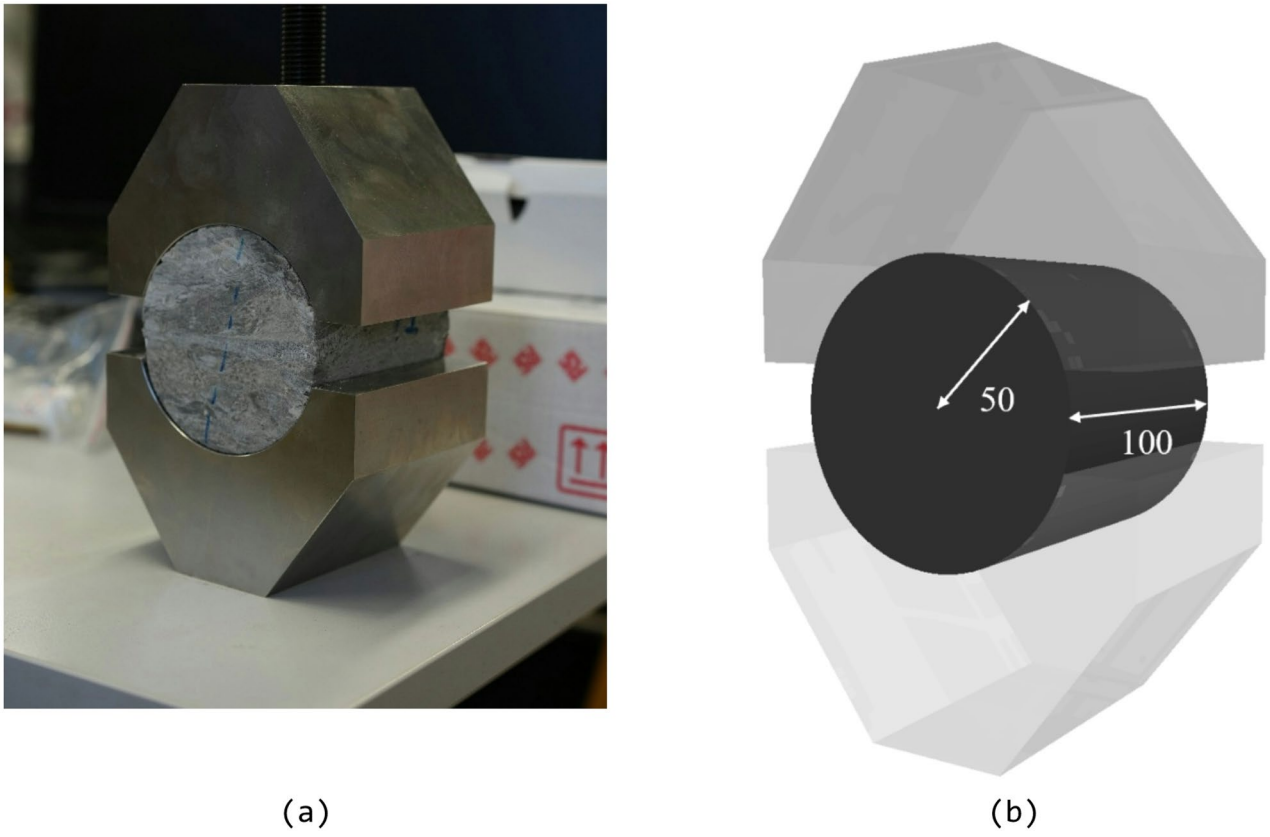

Fig. 3 Three-dimensional representation of specimen inside clamp system (**a**) Photograph, (**b**) Schematic [mm]

in a controlled temperature furnace at 230 °C for 3 h to degrade the adhesive. The residue was then removed easily by non-abrasive manual scraping, ensuring no damage to the metal fixture surface, thereby providing contaminant-free interfacial contact surfaces for subsequent tests.

3 Numerical model

To analyze the proposed testing scheme, 3-dimensional numerical simulations were conducted using FLAC^{3D}. The numerical model setup is shown in Fig. 4, which includes sample, metal clamps, glue and optional a central material interface. To ensure an accurate representation of the experimental process, interface elements (INS) were introduced between the upper and lower clamps and the rock specimen to simulate the mechanical behavior of the bonding layer. Additionally, interface elements (INC) can be assigned optionally centric between two materials to simulate for instance a rock-concrete interface or to test a bonding material (see Fig. 4).

A Mohr–Coulomb model with a tensile cut-off was adopted as a pragmatic engineering representation to capture brittle tensile failure at the specimen scale and to reproduce the peak load, failure location, and stress heterogeneity observed in the experiments. The model does not explicitly represent fracture-energy-controlled crack propagation or post-peak softening; therefore, the simulations are used here primarily to interpret stress distribution and failure initiation rather than detailed fracture mechanics.

For the clamps an isotropic elastic law was applied, because any kind of plastification or failure can be excluded. The elastic parameters correspond to the precisely defined material parameters of the metal clamps. For the tested material Mohr-Coulomb parameters were applied typical for salt rock, sandstone and a special concrete. The parameters for the interface representing the

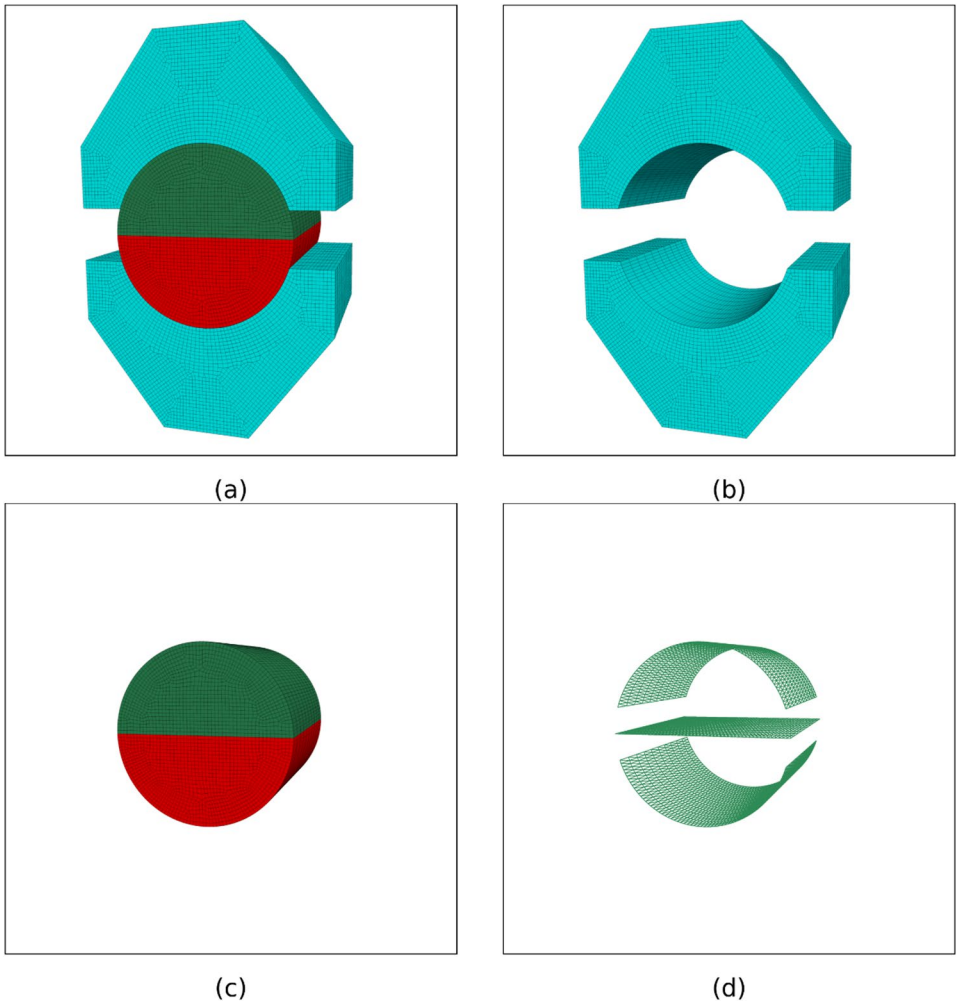

Fig. 4 Numerical model setup incl. mesh. **a** Clamps incl test material, **b** Metal clamps, **c** Test material with interface, **d** Interfaces representing glue and potential material interface

glue (INS) were taken according to the glue product data sheet (tensile strength and stiffness). Cohesion and friction at the interfaces are without relevance because the potential failure will be a pure tensile failure mode.

At first numerical simulations were performed assuming an isotropic and homogeneous rock specimen (sandstone) without an interface and with a tensile strength of 1.6 MPa. The used parameters are shown in Table 1. We duplicated the lab test procedure by applying the vertical loading velocity at the outer boundaries of the metal clamps and monitored the corresponding applied tensile force, the fracture evolution and identified the failure plane (tensile fracturing).

4 Validation for homogeneous material

A well investigated sandstone was used to validate the proposed test procedure. This sandstone (Postaer Sandstone "Alte Post, Erste Bank") has an uniaxial tensile strength (measured in classical direct tensile tests according to ISRM suggested methods (1978)) of 1.6 ± 0.6 MPa (47 samples). Figure 5 documents results according to the new proposed procedure.

For isotropic and homogeneous sample it was observed that crack propagation initiates near to the clamps (see Fig. 7) producing a nearly horizontal fracture (see Fig. 5), primarily due to stress concentrations inside the rock near to the clamps. Figure 6 presents the force-displacement curves of three specimens up to tensile failure (see also Fig. 6). The peak (failure) loads are 17.64 kN for Sample A, 18.15 kN for Sample B, and 15.69 kN for Sample C. The corresponding tensile strength values, calculated by dividing peak force by fracture area, all fall within the previously mentioned range of 1.6 ± 0.6 MPa. In this study, the nominal tensile strength is computed as

Table 1 Material parameters

Item	MgO-based concrete	Salt rock	Sandstone
Young's modulus (MPa)	30e3	20e3	30e3
Poisson's ratio	0.30	0.25	0.30
Cohesion (MPa)	15	2.5	10
Friction angle (°)	40.0	37.0	30.0
Tensile strength (MPa)	2.0	2.0	1.6
Density (kg/m3)	2500	2160	2500
Interface parameters	INC	INS	
Stiffness-normal (N/m)	10e9*	1e12	
Stiffness-shear (N/m)	3e9*	0.3e12	
Cohesion (MPa)	1.0*	10.0*	
Friction (°)	45.0*	45.0*	
Tensile strength (MPa)	1.0	1e9	
Metal clamp parameters			
Young's modulus (MPa)	210e3		
Poisson's ratio	0.28		
Density (kg/m^3)	7800		

*Rough estimation (however, unimportant for the specific tests under consideration)

$$\sigma_t = F_{max}/A_f,$$

where F_{max} is the peak tensile force and A_f is the final fracture area measured after testing. This indicates that the results obtained by this study are consistent with previously reported mechanical properties of this sandstone.

To investigate the behavior in more detail numerical simulations were performed. Due to symmetry conditions only the upper half of the experimental set-up was modelled to increase the computational speed.

As shown later in Fig. 3, the tensile stress distribution along the final tensile fracture plane is not homogeneous. Local peaks occur close to the clamps, which initiate the crack propagation already documented in Fig. 7. This inhomogeneous stress distribution makes the determination of tensile strength less accurate. However, for practical applications and under consideration of the general scatter of rock mechanical data this level of accuracy may be sufficient. Therefore, for homogeneous specimens the obtained value should be interpreted as a conservative estimate under the present boundary conditions (i.e., a lower bound), rather than an exact representation of an ideally uniform uniaxial tensile strength.

5 Validation for composite material (material with interface)

Exemplary, the tensile strength of the interface of a composite material (salt rock and MgO-based concrete) was determined. Figure 8 shows the sample before and after testing. Material parameters are given already in Table 1. The numerical model for simulating the test contains an interface between the two materials. The interface tensile strength was determined by the new proposed test procedure and the numerical simulation is used to duplicate the lab test. The material interface has a much lower tensile strength compared with the two materials in contact. Therefore, the tensile failure develops along the interface as illustrated in detail by Fig. 8 (lab) and Fig. 9 (numerical model). The corresponding force-displacement curves of two lab tests are shown in Fig. 10. By investigating the numerical simulation, it becomes obvious that the tensile stress distribution along the interface is nearly, but not absolutely perfect homogeneous (see Fig. 3).

To investigate the tensile failure behavior in more detail the evolution of tensile stresses up to failure were analyzed by numerical simulations. For the intact homogeneous sample, due to the symmetry, only the upper half of the experimental set-up was modelled (see Figs. 7 and 13). Tests with central interface were modelled using the complete experimental set-up (see Figs. 4 and 9). The evolution of tensile stresses was monitored along line A (intact homogeneous sample) and line B (composite material with interface). These scanlines (see Fig. 11) mark the final tensile fracture planes. Figures 12 and 13

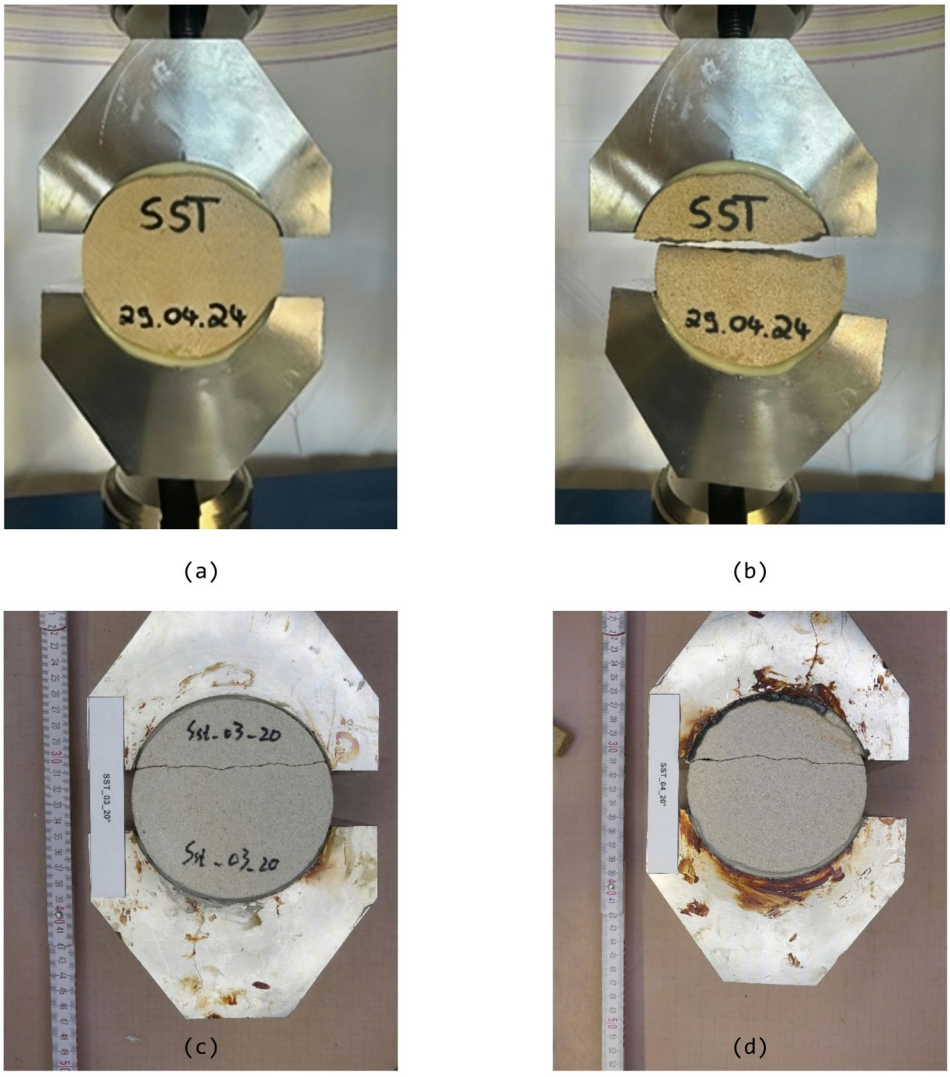

Fig. 5 Sandstone sample before (**a**) and after (**b**-**d**) direct tensile tests

illustrate the force-displacement curves for these two types of tests. Some points are marked in these figures, for which the stress profiles along the scanlines are illustrated in Fig. 14. Figure 14 shows, that tensile stresses developing along a central weak plane (interface) are nearly perfect homogeneous in contrast to the homogeneous model, where peak stresses develop close to the clamps. The tensile strength of the interface can simply be calculated by dividing the peak force by the final fracture area.

These results confirm that the proposed tensile test method provides a reliable approach for determining interface tensile strength in composite materials. However, prerequisite is, that the interface tensile strength is significantly lower than the tensile strength of the two materials. Figure 3 documents also that the orientation of the maximum tensile stress along the scanline is vertical in agreement with the loading direction. If the interface tensile strength is comparable to that of the adjacent materials, failure may shift to the bulk material or to regions influenced by end effects, and the peak-load-based nominal strength should not be interpreted as an interface property.

Experimental and numerical results exhibit good agreement. Upon reaching peak stress, the force-displacement curves suddenly drop, indicating an abrupt failure when reaching the tensile strength (brittle failure mode). Table 2 summarizes the results.

The results of lab tests and numerical simulations (see Table 2) for the composite material interface (salt rock and MgO-based concrete) reveal a high degree of consistency with deviation of only 0.8% and 3.7%, respectively.

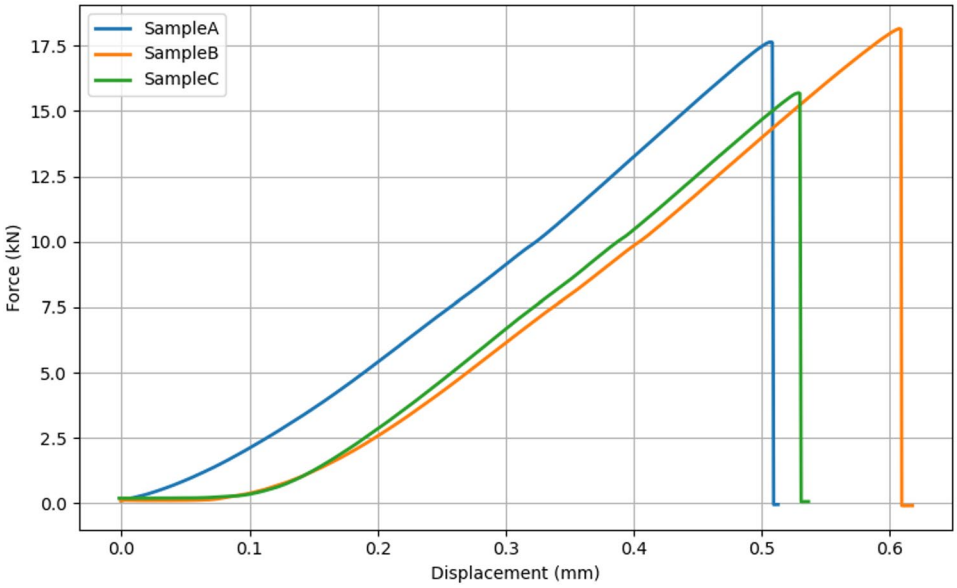

Fig. 6 Force-displacement curves of sandstone samples obtained by lab test (see Fig. 5)

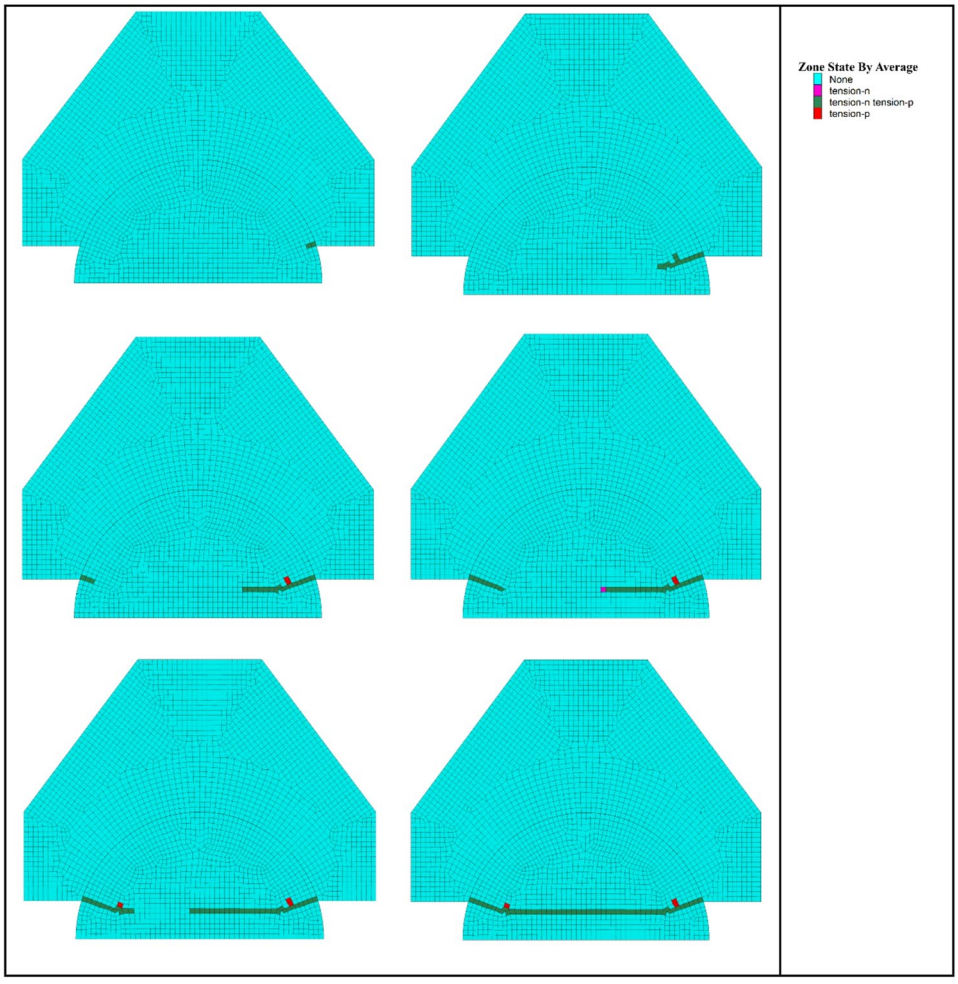

Fig. 7 Evolution and spatial distribution of fracture evolution (tensile failure) for selected loading stages (The loading direction is vertical)

Fig. 8 Composite sample (MgO-based concrete and salt rock) before (left) and after (right) direct tensile test (sample D, see also Table 2)

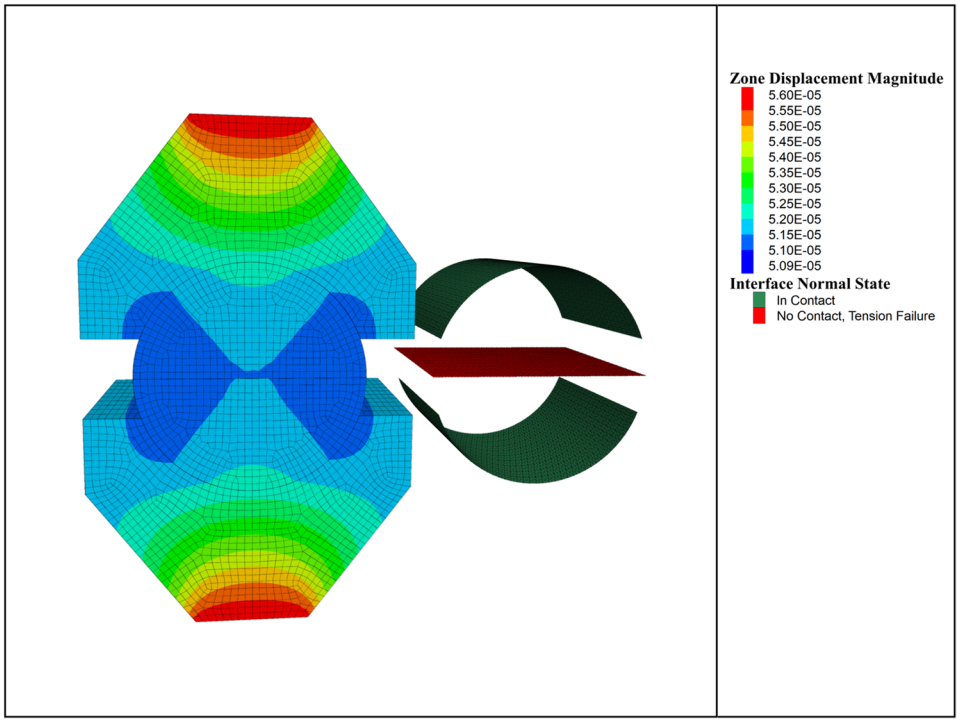

Fig. 9 Displacement magnitude [m] (left) and contact state (right) of the interfaces at the point in time of sample failure (sample D)

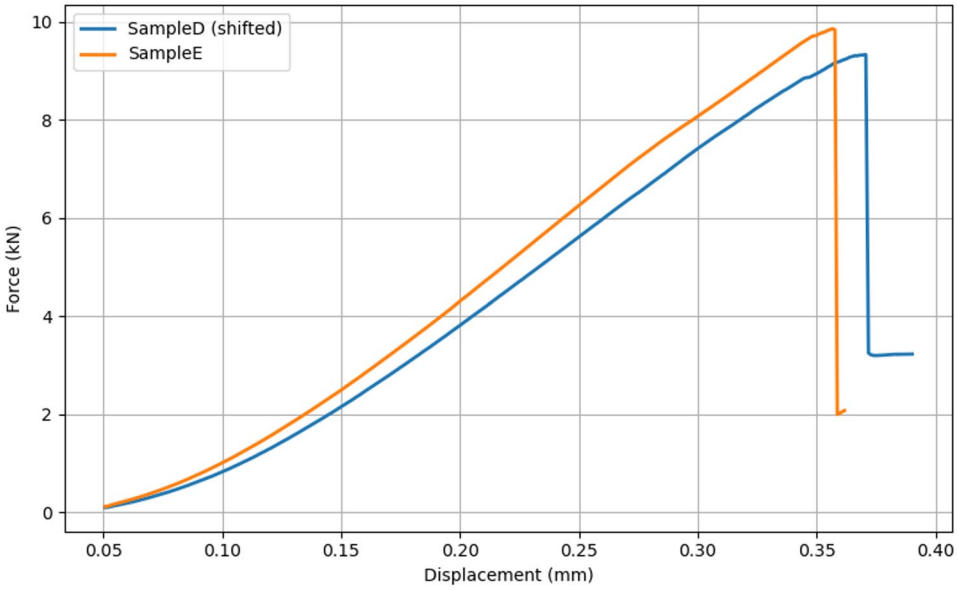

Fig. 10 Force-displacement curve obtained by lab tests for rock-concrete sample

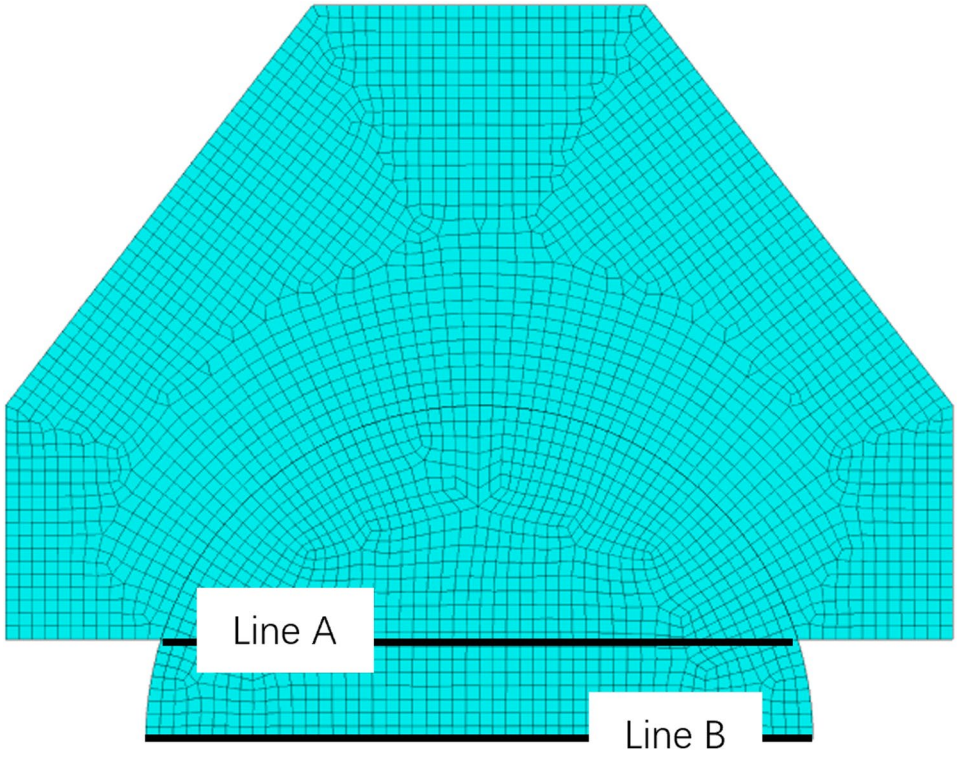

Fig. 11 Numerical model with indication of scanlines used in Fig. 14

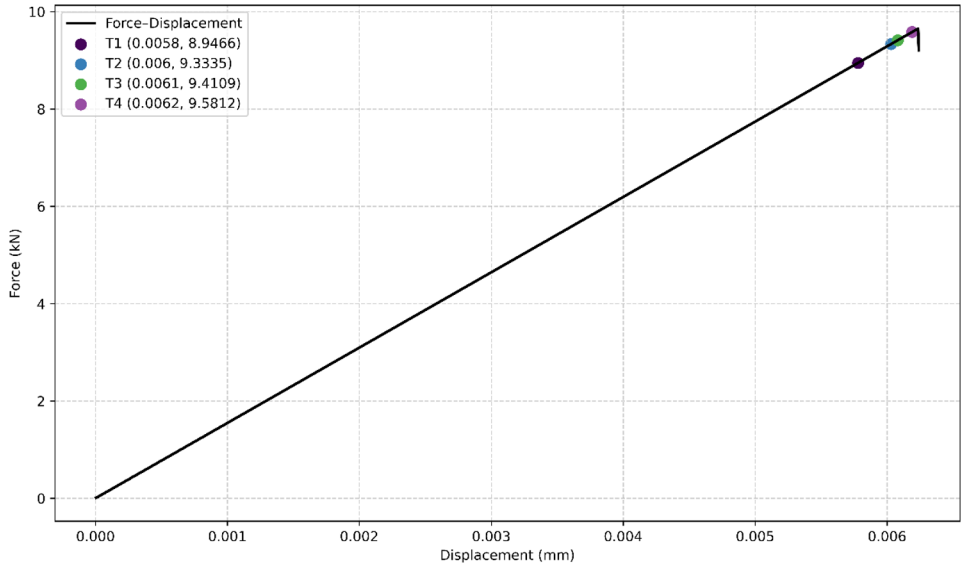

Fig. 12 Force-displacement curves with four marked loading stages (T1-T4) obtained by numerical simulation (homogeneous materials)

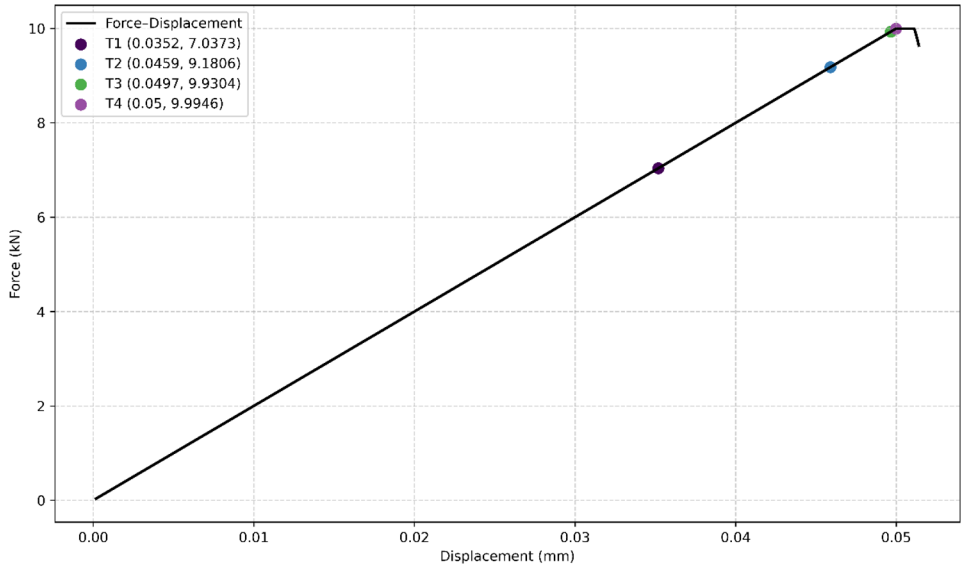

Fig. 13 Force-displacement curves with four marked loading stages (T1-T4) obtained by numerical simulation (composite materials)

6 Comparison with established direct tensile tests and applicability

Compared with established direct tensile arrangements following ISRM/ASTM concepts (bonded end caps and seating/linkage systems), the proposed clamp-based procedure mainly differs in the load-transfer path and the targeted specimen configurations. It is intended for cases where standard end-capping approaches are difficult to apply, namely short cylindrical specimens ($L/D \approx 1$) and composite specimens containing an axial interface/weak plane requiring controlled failure localization.

For intact homogeneous rocks, end effects may lead to stress peaks near the clamps (Fig. 3) and crack initiation outside the specimen mid-plane; thus the measured nominal strength is interpreted conservatively as a lower bound. For interface-dominated composite specimens with a sufficiently weak interface, the tensile stress along the interface becomes much more uniform (Fig. 3), enabling a practical determination of interface tensile strength.

The present study is intended as a technical guideline and proof-of-concept; broader validation, repeatability assessment and bias quantification will be addressed in future work.

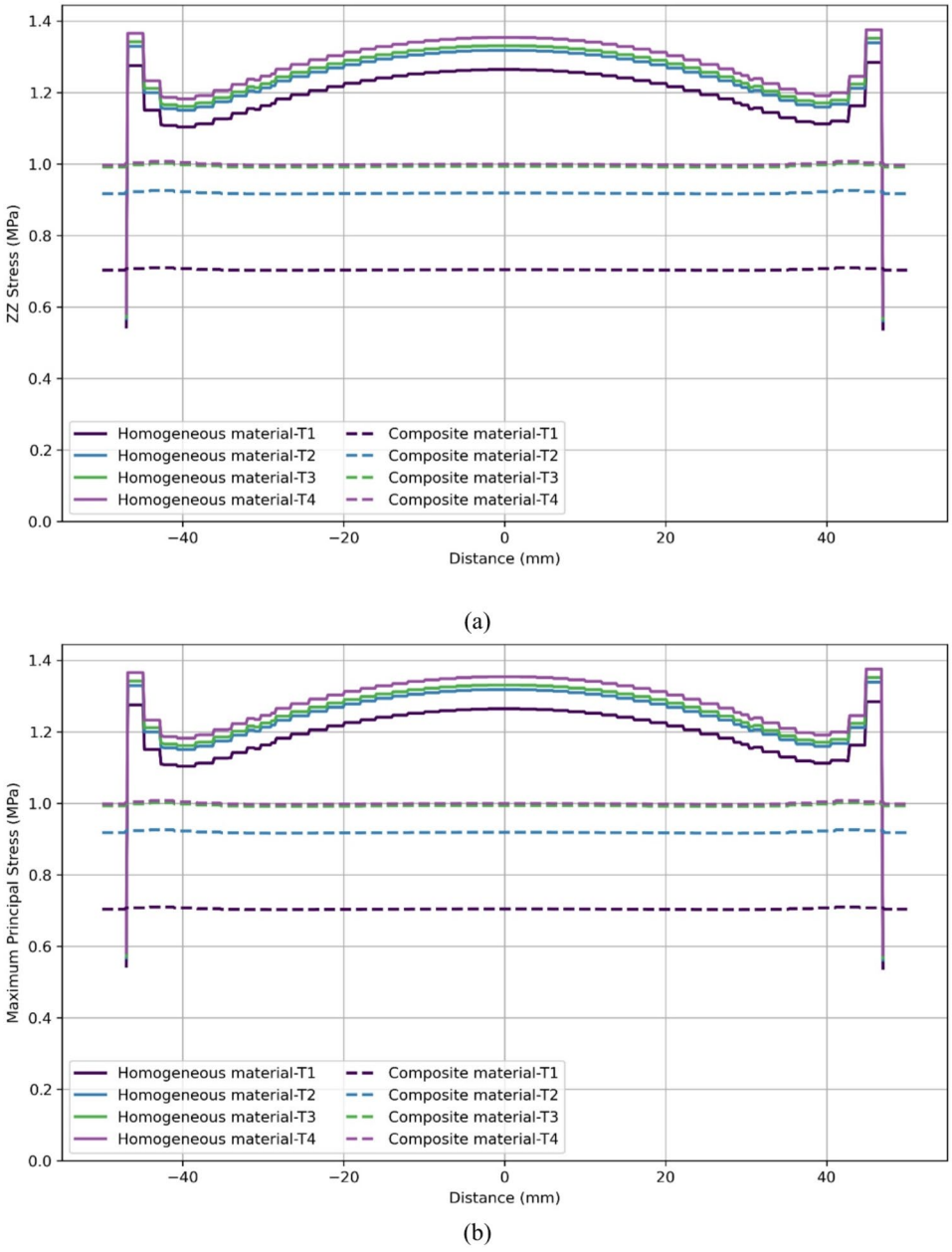

Fig. 14 Numerical simulation results: Vertical stress component (**a**) and maximum tensile stress (**b**) along scanline A for homogeneous material and scanline B for composite material (see Fig. 11)

7 Conclusions

The proposed new test procedure is well suited to determine the direct tensile strength of interfaces located centric inside the sample, but allows also the determination of a lower bound (conservative value) for homogeneous materials. In both cases the measured peak load has to be divided by the final fracture area.

The proposed method overcomes specific challenges associated with traditional direct tensile tests, such as demands on sample geometry by allowing testing on shorter samples and especially those with interfaces (composite materials of material with intrinsic interface). The procedure is verified and validated by experimental testing and numerical simulations, demonstrating its effectiveness and reliability. By appropriate design of the clamps also samples with other diameter can be used. The tests are easy to perform and the sample holder can be used repeatedly without bigger efford.

Table 2 Summary of results (lab test vs. numerical simulations)

Sample data and measured values	Salt rock - concrete Sample D	Salt rock - concrete Sample E
Diameter (mm)	100.64	99.33
Length (mm)	98.83	98.02
Interface surface (mm^2)	9946.25	9736.33
Aspect ratio (L/D)	0.98	0.99
Fracture surface area (mm^2)	9946.25	9736.33
Experimental fracture load (kN)	9.86	9.33
Simulated fracture load (kN)	9.94	9.69
Fracture load deviation (%)	0.8	3.7
Experimental tensile strength (MPa)	0.991	0.958
Numerical tensile strength (MPa)	0.999	0.995

For homogeneous specimens, the measured nominal strength should be interpreted conservatively as a lower bound due to end effects. For interface specimens, applicability is strongest when the interface is significantly weaker than the adjacent materials; otherwise, failure may shift away from the interface. The present dataset for interface testing is limited, and broader validation and repeatability assessment will be addressed in future work.

Authors' contributions

M.F. and H.K. conceived the study and designed the overall research plan. Y.D. led the investigation, performed the experiments and numerical analyses, and wrote the first draft of the manuscript. A.M. contributed to the numerical simulations. T.W. assisted with the laboratory measurements. M.F., H.K., A.M. and T.W. reviewed and revised the manuscript. All authors read and approved the final manuscript.

Data availability

No datasets were generated or analysed during the current study.

Declarations

Competing interests

The authors declare no competing interests. Heinz Konietzky is a member of the editorial board of this journal.

Received: 11 December 2025 / Revised: 17 March 2026 / Accepted: 19 March 2026
Published online: 23 April 2026

References

1. Alzo'ubi AK, Martin CD, Cruden DM (2010) Influence of tensile strength on toppling failure in centrifuge tests. Int J Rock Mech Min Sci 47:974–982. https://doi.org/10.1016/j.ijrmms.2010.05.011
2. Liang Z, Xue R, Xu N, Dong L, Zhang Y (2020) Analysis on microseismic characteristics and stability of the access tunnel in the main powerhouse, Shuangjiangkou hydropower station, under high in situ stress. Bull Eng Geol Environ 79:3231–3244. https://doi.org/10.1007/s10064-020-01738-6
3. Graue B, Siegesmund S, Middendorf B (2011) Quality assessment of replacement stones for the Cologne Cathedral: mineralogical and petrophysical requirements. Environ Earth Sci 63:1799–1822. https://doi.org/10.1007/s12665-011-1077-x
4. Klanphumeesri S (2010) Direct tension testing of rock specimens. Master of Engineering thesis, Suranaree University of Technology, Nakhon Ratchasima
5. Tavallali A, Vervoort A (2010) Failure of layered sandstone under Brazilian test conditions: effect of micro-scale parameters on macro-scale behaviour. Rock Mech Rock Eng 43:641–653. https://doi.org/10.1007/s00603-010-0084-7
6. Markides CF, Pazis DN, Kourkoulis SK (2012) The Brazilian disc under non-uniform distribution of radial pressure and friction. Int J Rock Mech Min Sci 50:47–55. https://doi.org/10.1016/j.ijrmms.2011.12.012
7. Erarslan N, Williams DJ (2012) Experimental, numerical and analytical studies on tensile strength of rocks. Int J Rock Mech Min Sci 49:21–30. https://doi.org/10.1016/j.ijrmms.2011.11.007
8. Li D, Wong LNY (2013) The Brazilian disc test for rock mechanics applications: review and new insights. Rock Mech Rock Eng 46:269–287. https://doi.org/10.1007/s00603-012-0257-7
9. Dan DQ, Konietzky H, Herbst M (2013) Brazilian tensile strength tests on some anisotropic rocks. Int J Rock Mech Min Sci 58:1–7. https://doi.org/10.1016/j.ijrmms.2012.08.010
10. Loukil M, Hassine WB, Limam O, Kotronis P (2019) Experimental determination of GFRC tensile parameters from three-point bending tests using an analytical damage model. Constr Build Mater 223:477–490. https://doi.org/10.1016/j.conbuildmat.2019.07.005
11. Liao Z, Zhu J, Tang C (2019) Numerical investigation of rock tensile strength determined by direct tension, Brazilian and three-point bending tests. Int J Rock Mech Min Sci 115:21–32. https://doi.org/10.1016/j.ijrmms.2019.01.007
12. Liu J, Wu Y, Liu J, He Y, Shen X, Du Y, Sun B (2025) Acoustic emission evolution and fracture mechanism of rock for direct tensile failure. Int J Rock Mech Min Sci 185:105974. https://doi.org/10.1016/j.ijrmms.2024.105974
13. Liu J, Lyu C, Lu G, Shi X, Li H, Liang C, Deng C (2022) Evaluating a new method for direct testing of rock tensile strength. Int J Rock Mech Min Sci 160:105258. https://doi.org/10.1016/j.ijrmms.2022.105258
14. Aliha MRM, Ebneabbasi P, Karimi HR, Nikbakht E (2021) A novel test device for the direct measurement of tensile strength of rock using ring-shaped sample. Int J Rock Mech Min Sci 139:104649. https://doi.org/10.1016/j.ijrmms.2021.104649
15. ISRM (1978) Suggested methods for determining tensile strength of rock materials. Int J Rock Mech Min Sci Geomech Abstr 15:99–103. https://doi.org/10.1016/0148-9062(78)90003-7
16. ASTM International (2020) Standard test method for direct tensile strength of intact rock core specimens (D2936-20). ASTM International, West Conshohocken
17. Pérez-Rey I, Muñiz-Menéndez M, Frühwirt T, Konietzky H, Jacobsson L, Perras MA, Atefi-Monfared K, Mas Ivars D, Sánchez Juncal A, Alejano LR (2024) Assessment of direct tensile strength tests in rock through a multi-laboratory benchmark experiment. Rock Mech Rock Eng 57:3617–3634. https://doi.org/10.1007/s00603-023-03751-z

Publisher's note